nature structural & molecular biology

Conformational selection of translation initiation factor 3 signals proper substrate selection

Margaret M Elvekrog[1,2] & Ruben L Gonzalez Jr[1]

During translation, initiation factor 3 (IF3) binds to the small (30S) ribosomal subunit and regulates the fidelity with which the initiator tRNA and mRNA start codon substrates are selected into the 30S initiation complex (30S IC). The molecular mechanism through which IF3 promotes the recognition and signaling of correct substrate selection, however, remains poorly defined. Using single-molecule fluorescence resonance energy transfer, we show that 30S IC–bound *Escherichia coli* IF3 exists in a dynamic equilibrium between at least three conformations. We found that recognition of a proper anticodon-codon interaction between initiator tRNA and the start codon within a completely assembled 30S IC selectively shifts this equilibrium toward a single conformation of IF3. Our results strongly support a conformational selection model in which the conformation of IF3 that is selectively stabilized within a completely and correctly assembled 30S IC facilitates further progress along the initiation pathway.

Translation initiation, the rate-limiting step of protein synthesis and a major regulatory checkpoint in gene expression[1], involves multistep, initiation factor–mediated assembly of a 70S IC that contains an initiator *N*-formylmethionyl–tRNA (fMet-tRNA^{fMet}) and a mRNA start codon within the P (peptidyl-tRNA binding) site of the 70S IC (**Fig. 1a**)[1]. The accuracy of fMet-tRNA^{fMet} and start-codon selection is crucial, as selection of an elongator aminoacyl-tRNA (aa-tRNA) or a noncanonical start codon during 70S IC assembly can result in proteins harboring an incorrect N-terminal amino acid or translation of a frameshifted mRNA. The fidelity of translation initiation is established primarily through the cooperative biochemical activities of three essential initiation factors: IF1, IF2 and IF3 (ref. 1). Extensive biochemical studies have suggested that IF3 has a negative regulatory role in ensuring the accuracy of translation initiation by uniformly destabilizing the binding of all tRNAs at the 30S IC P site[2] and selectively inhibiting the joining of 50S subunits onto 30S ICs carrying either elongator aa-tRNAs[2–4] or an fMet-tRNA^{fMet} containing mismatched base pairs to a noncanonical start codon[5]. Despite these biochemical studies, however, a structure-based understanding of how IF3 recognizes and signals fMet-tRNA^{fMet} and start-codon selection within the 30S IC to regulate further progress along the initiation pathway remains elusive.

IF3 comprises globular N-terminal and C-terminal domains (designated the NTD and CTD, respectively) connected by a flexible interdomain linker of highly conserved length and amino acid character[6] that enables IF3 to dynamically sample a broad range of interdomain conformations when free in solution[7] (**Fig. 1b**). Whether 30S IC–bound IF3 has similar conformational dynamics and whether these dynamics have a role in the fidelity function of IF3 within the 30S IC, however, remains unknown. Unfortunately, high-resolution structural information on the 30S IC is lacking, and attempts to localize the IF3 binding site on the 30S IC have reached conflicting conclusions, particularly regarding the placement of the IF3 NTD on the 30S IC[8–10]. At least one of the proposed IF3 binding sites is expected to sterically block formation of one of the key intersubunit bridges that connect the two ribosomal subunits within a 70S IC, thereby providing an attractive structural model for the subunit anti-association activity of IF3[8,9]. On their own, however, structural models such as this do not account for the selective relaxation of the subunit anti-association activity of IF3 after correct substrate selection as an fMet-tRNA^{fMet}– and start codon–dependent repositioning of IF3 on the 30S IC and/or dissociation of IF3 from the 30S IC[2,11] would be required to facilitate access to the 30S IC intersubunit bridge components that are otherwise blocked by IF3.

To determine whether IF3 is conformationally dynamic on the 30S IC and investigate whether these dynamics have a role in the fMet-tRNA^{fMet}– and start codon–dependent relaxation of the subunit anti-association activity of IF3, we developed an intramolecular IF3 fluorescence resonance energy transfer (FRET) signal that reports on relative distance changes between the IF3 NTD and CTD. Using single-molecule FRET (smFRET), we found that 30S IC–bound IF3 samples and interconverts between at least three distinct FRET states, demonstrating that IF3 exists in a conformational equilibrium on the 30S IC. By conducting smFRET experiments on a series of 30S ICs, we show that the presence of either or both of the other initiation factors, IF1 and IF2, on the 30S IC can modulate the conformational equilibrium of 30S IC–bound IF3. Most notably, however, we demonstrate that the presence and identities of the tRNA and codon that are positioned within the P site of the 30S IC can also modulate the conformational equilibrium of 30S IC–bound IF3 such that the presence of an initiator tRNA and start codon uniquely shifts the equilibrium toward a single conformation of IF3. We use our results, integrated with the available biochemical data, to propose a

[1]Department of Chemistry, Columbia University, New York, New York, USA. [2]Present address: Department of Biochemistry and Biophysics, University of California, San Francisco, San Francisco, California, USA. Correspondence should be addressed to R.L.G. (rlg2118@columbia.edu).

Received 8 August 2012; accepted 5 March 2013; published online 14 April 2013; doi:10.1038/nsmb.2554

conformational selection model in which the conformation of IF3 that is uniquely stabilized within a completely and correctly assembled 30S IC facilitates further progress along the initiation pathway, whereas alternative conformations of IF3 are inhibitory.

RESULTS

Development of a functional, dual fluorescently labeled IF3

Labeling of an IF3 mutant carrying one cysteine at its NTD and one cysteine at its CTD with Cy3 FRET donor and Cy5 FRET acceptor fluorophores and subsequent purification generated a dual Cy3-Cy5–labeled IF3 ($IF3^{C65S\ S38C\ K97C}$(Cy3-Cy5), hereafter referred to as IF3(Cy3-Cy5)) (**Fig. 1b** and **Supplementary Fig. 1**) that retained near–wild type biochemical function (**Supplementary Fig. 2**). Using 5′-biotinylated mRNAs, we assembled 30S ICs carrying IF3(Cy3-Cy5), tethered them to the polyethylene glycol–passivated and streptavidin-derivatized surface of a quartz microfluidic flow cell and imaged them at single-molecule resolution using a total internal reflection fluorescence (TIRF) microscope operating at an acquisition rate of 10 frames s^{-1} (ref. 12). Control experiments demonstrated that under our experimental conditions, 80–95% of the individual, surface-localized IF3(Cy3-Cy5)s were bound to the flow cell surface by their interaction with a 30S IC carrying a biotinylated mRNA (**Supplementary Fig. 3**). For further details regarding sample preparation, TIRF imaging, control experiments and data analyses, see the **Supplementary Note**.

30S IC–bound IF3 is conformationally dynamic

We designed our initial experiments to probe the conformation of IF3 bound to a 30S subunit in the absence of the other initiation factors and tRNA (30S $IC^{-tRNA}_{-1/-2}$, where the −tRNA superscript and −1/−2 subscript denote the lack of a tRNA within the P site and the lack of IF1 and IF2, respectively). The resulting smFRET efficiency (E_{FRET}) versus time trajectories sampled three distinct FRET states centered at E_{FRET} values of 0.23 ± 0.01, 0.42 ± 0.01 and 0.87 ± 0.01, with 29.9% ± 8.6% of the trajectories showing fluctuations between at least two FRET states before photobleaching and 70.1% ± 17.3% of the trajectories sampling only one of these FRET states before photobleaching (**Fig. 2a** and **Supplementary Fig. 4**). Assuming rapid, isotropic tumbling of one or both fluorophore transition dipoles and a Förster radius of ~55 Å for the Cy3-Cy5 FRET pair[12,13], we interpret the E_{FRET} values of 0.23, 0.42 and 0.87 (**Supplementary Table 1**) as corresponding to interdomain distances of ~67 Å, ~58 Å and ~40 Å, respectively. Notably, this range of distances is consistent with the interdomain distances accessible to IF3 when free in solution (28–65 Å)[7]. Hereafter, we refer to the conformations of 30S IC–bound IF3 that are associated with each of these E_{FRET} values and distances as extended ($IF3_{ext}$ (0.23 and ~67 Å)), intermediate ($IF3_{int}$ (0.42 and ~58 Å)) and compact ($IF3_{cpt}$ (0.87 and ~40 Å)). Thermodynamic and kinetic analyses of the trajectories revealed equilibrium fractional occupancies of 54% ± 9%, 40% ± 10% and 6% ± 2% for $IF3_{ext}$, $IF3_{int}$ and $IF3_{cpt}$, respectively (**Supplementary Table 2**), and estimated the rates of interconversions between the three IF3 conformations as ranging between 0.002 and 0.11 s^{-1} (**Supplementary Table 3**). Interpreted within the context of previously reported *in vitro* subunit joining experiments demonstrating that 30S ICs analogous to 30S $IC^{-tRNA}_{-1/-2}$ are substantially inhibited in their ability to undergo subunit joining[4], these data suggest that $IF3_{ext}$ and $IF3_{int}$ are conformations of IF3 that are not conducive to rapid 50S subunit joining.

It is unlikely that the interdomain dynamics of IF3 that we found here arise from a scenario in which one IF3 domain is tightly bound to the 30S IC and the other IF3 domain remains free in solution, undergoing restricted diffusion through the interdomain linker. Dynamic exchange between different interdomain conformations of IF3 involving such restricted diffusion of a free IF3 domain would be expected to occur with rates that are 7–11 orders of magnitude faster than our estimated rates of interconversions between $IF3_{ext}$, $IF3_{int}$ and $IF3_{cpt}$[14]. Instead, we propose a scenario in which both IF3 domains can bind to the 30S IC and exchange between different interdomain conformations as a result of (i) active repositioning of one or both IF3 domains among several binding sites on the 30S IC; (ii) passive changes in the distance between the two IF3 domains resulting from dynamic rearrangements of the 30S IC; or (iii) a combination of (i) and (ii). To test whether IF3 actively or passively participates in the dynamics, we constructed

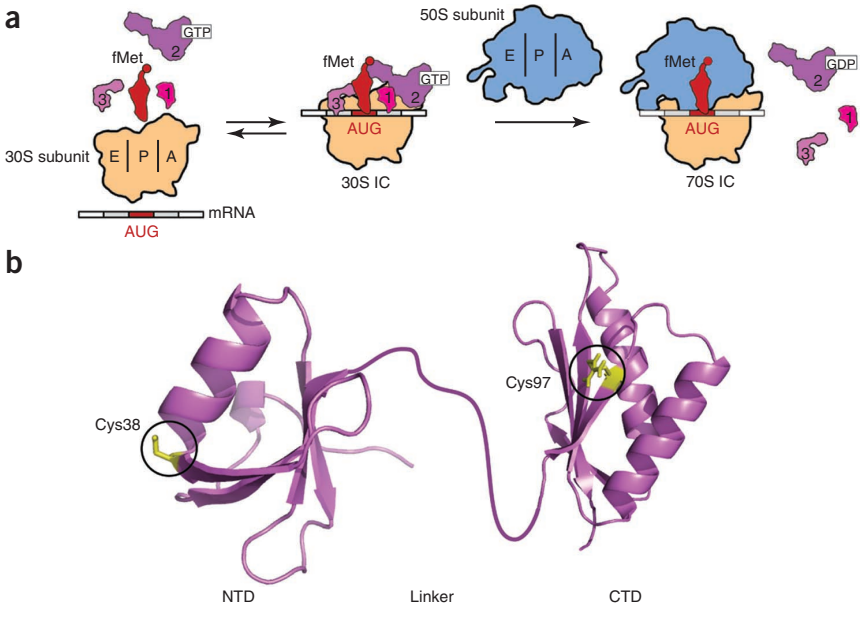

Figure 1 Translation initiation in bacteria and fluorescent labeling of IF3. (**a**) A minimal model of translation initiation. 30S IC refers to a completely and correctly assembled 30S ribosomal initiation complex, and 70S IC refers to a 70S ribosomal initiation complex harboring an initiator fMet-$tRNA^{fMet}$ bound to an AUG start codon at the P site. The initiation factors, mRNA and fMet-$tRNA^{fMet}$ reversibly bind to the 30S ribosomal subunit to form the 30S IC[17]. Subsequent joining of the 50S subunit to the 30S IC triggers GTP hydrolysis by IF2 and, ultimately, dissociation of the three initiation factors. E, P and A indicate the tRNA exit (E), peptidyl-tRNA binding (P) and aminoacyl-tRNA binding (A) sites on the 30S and 50S subunits. The numerals 1, 2 and 3 indicate IF1, IF2 and IF3, respectively. (**b**) X-ray crystal structures of the NTD (Protein Data Bank (PDB) ID 1TIF) and CTD (PDB ID 1TIG) of IF3 from *Bacillus stearothermophilus*. The linker connecting the NTD and CTD was cartooned by hand. The residues on the *B. stearothermophilus* structures corresponding to those in a C65S, S38C and K97C triple mutant of *E. coli* IF3 that was prepared and fluorescently labeled with Cy3 and Cy5 at Cys38 and Cys97 are indicated in the depicted structure.

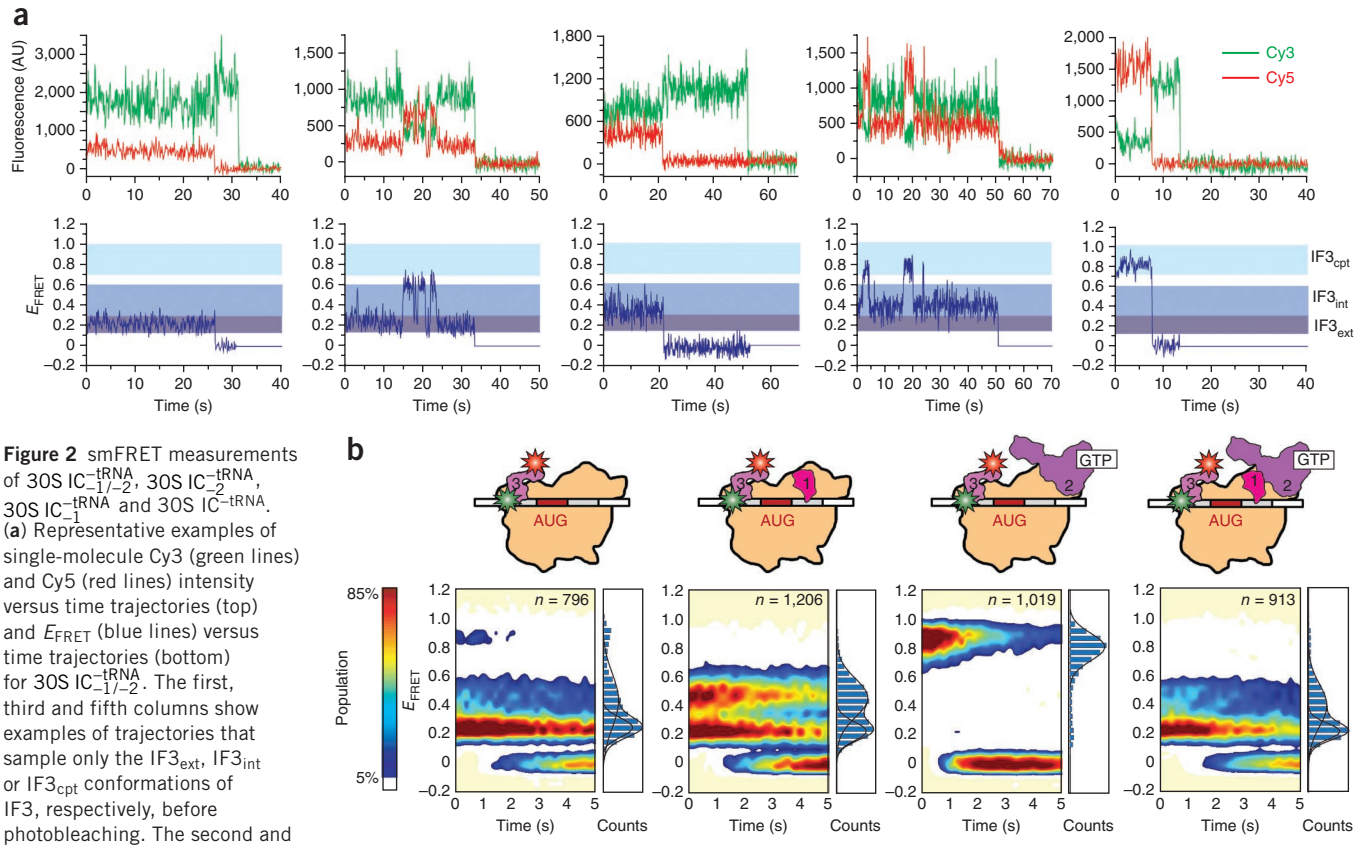

Figure 2 smFRET measurements of 30S $IC^{-tRNA}_{-1/-2}$, 30S IC^{-tRNA}_{-2}, 30S IC^{-tRNA}_{-1} and 30S IC^{-tRNA}. (**a**) Representative examples of single-molecule Cy3 (green lines) and Cy5 (red lines) intensity versus time trajectories (top) and E_{FRET} (blue lines) versus time trajectories (bottom) for 30S $IC^{-tRNA}_{-1/-2}$. The first, third and fifth columns show examples of trajectories that sample only the $IF3_{ext}$, $IF3_{int}$ or $IF3_{cpt}$ conformations of IF3, respectively, before photobleaching. The second and fourth columns show examples of trajectories that fluctuate between the $IF3_{ext}$ and $IF3_{int}$ conformations of IF3 and the $IF3_{int}$ and $IF3_{cpt}$ conformations of IF3, respectively, before photobleaching. AU, arbitrary units. (**b**) Two-dimensional surface contour plots of the time evolution of the population FRET for 30S $IC^{-tRNA}_{-1/-2}$, 30S IC^{-tRNA}_{-2}, 30S IC^{-tRNA}_{-1} and 30S IC^{-tRNA}. The *n* values shown are the total number of E_{FRET} versus time trajectories that were used to construct each histogram. To the right of each contour plot is a normalized one-dimensional E_{FRET} histogram for the first 0.5 s of the E_{FRET} versus time trajectories comprising each data set. The cartoon above each surface contour plot and E_{FRET} histogram shows the composition of the 30S IC corresponding to the surface contour plot and E_{FRET} histogram.

an IF3(Cy3-Cy5) mutant that carries a single tyrosine-to-asparagine substitution at residue 75 (Y75N) within the interdomain linker ($IF3^{C65S\,S38C\,K97C\,Y75N}$(Cy3-Cy5), hereafter referred to as $IF3^{Y75N}$(Cy3-Cy5))[15]. Previous studies have shown that the Y75N mutation perturbs the fMet-$tRNA^{fMet}$– and start codon–selection activity of IF3 but doesn't affect its ability to bind to 30S subunits[15], biochemical properties that were recapitulated by our $IF3^{Y75N}$(Cy3-Cy5) construct (**Supplementary Fig. 2**). Comparison of smFRET data recorded using IF3(Cy3-Cy5) and $IF3^{Y75N}$(Cy3-Cy5) on otherwise identical 30S ICs and under otherwise identical experimental conditions revealed that the Y75N mutation appreciably alters the conformational equilibrium of IF3 (**Supplementary Figs. 3** and **5**). That a substitution mutation within the interdomain linker of IF3 can alter the dynamics we observed here demonstrates that IF3 has an active role in modulating the conformational equilibrium between $IF3_{ext}$, $IF3_{int}$ and $IF3_{cpt}$ regardless of whether these dynamics originate from the repositioning of IF3 domains on a static 30S IC, from structural rearrangements of the 30S IC itself, or both. Furthermore, the fact that $IF3^{Y75N}$(Cy3-Cy5) has impaired fMet-$tRNA^{fMet}$– and start codon–selection activity (**Supplementary Fig. 2**) suggests a functional link between the dynamics we observed here and the fidelity function of IF3.

IF1 and IF2 modulate the conformational equilibrium of IF3

Because IF1 amplifies and IF2 counteracts the tRNA-dissociation and subunit anti-association activities of IF3 during translation initiation[2], we investigated the effects of IF1 and IF2 on the conformational dynamics of 30S IC–bound IF3 by assembling and imaging 30S ICs in the presence of IF1 (30S IC^{-tRNA}_{-2}), IF2 (30S IC^{-tRNA}_{-1}) or both IF1 and IF2 (30S IC^{-tRNA}) (**Fig. 2b**). We imaged 30S ICs carrying IF1 and/or IF2 under saturating, 1 μM concentrations of each of these components. Relative to 30S $IC^{-tRNA}_{-1/-2}$, the presence of IF1 slightly shifted the conformational equilibrium of 30S IC^{-tRNA}_{-2}–bound IF3 away from $IF3_{ext}$ and $IF3_{cpt}$ and toward $IF3_{int}$, yielding fractional occupancies of 45% ± 3% ($IF3_{ext}$), 52% ± 3% ($IF3_{int}$) and 3% ± 1% ($IF3_{cpt}$) (**Fig. 2b** and **Supplementary Table 2**). In contrast, relative to 30S $IC^{-tRNA}_{-1/-2}$, the presence of IF2 markedly shifted the conformational equilibrium of 30S IC^{-tRNA}_{-1}–bound IF3 away from $IF3_{ext}$ and $IF3_{int}$ and toward $IF3_{cpt}$, yielding fractional occupancies of 23% ± 17% ($IF3_{ext}$), 11% ± 4% ($IF3_{int}$) and 66% ± 17% ($IF3_{cpt}$) (**Fig. 2b** and **Supplementary Table 2**). Notably, the effect of IF2 on the conformational equilibrium of 30S IC–bound IF3 was almost completely suppressed when IF1 was included together with IF2 in 30S IC^{-tRNA} (**Fig. 2b** and **Supplementary Table 2**). Thus, in the most physiologically relevant scenario in which all three initiation factors are present on the 30S IC[16], the conformational equilibrium of 30S IC^{-tRNA}–bound IF3 favors $IF3_{ext}$ and $IF3_{int}$ almost exclusively, yielding fractional occupancies of 56% ± 7% ($IF3_{ext}$), 42% ± 6% ($IF3_{int}$) and 2% ± 1% ($IF3_{cpt}$) (**Fig. 2b** and **Supplementary Table 2**) and transition rates that were similar to those observed for 30S $IC^{-tRNA}_{-1/-2}$ (**Supplementary Table 3**).

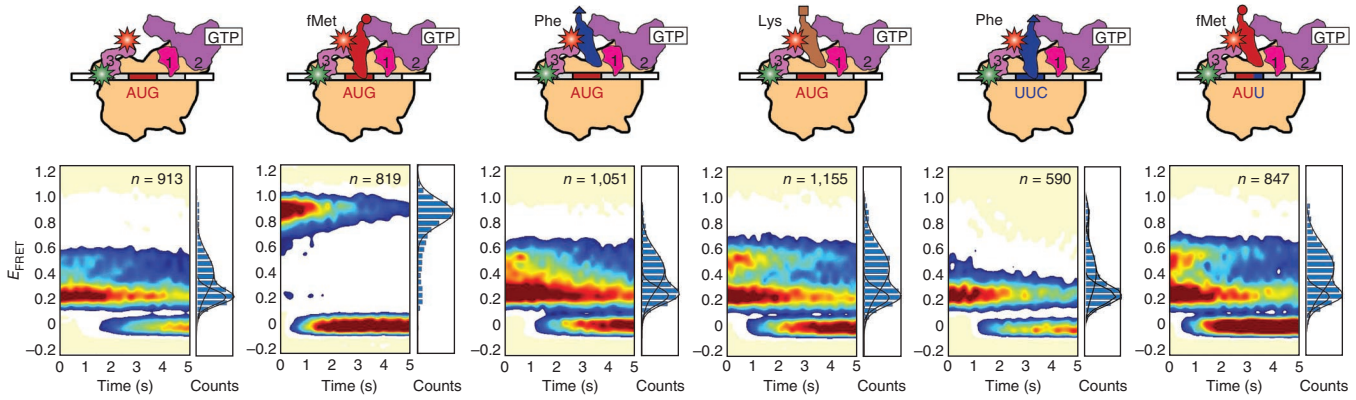

Figure 3 smFRET measurements of 30S IC^{-tRNA}, 30S IC^{fMet}, 30S IC^{Phe}, 30S IC^{Lys}, 30S IC^{Phe,UUC} and 30S IC^{fMet,AUU}. Data are displayed as in **Figure 2b**.

fMet-tRNA^{fMet} shifts the equilibrium toward IF3$_{cpt}$

A completely and correctly assembled 30S IC that is primed for rapid 50S subunit docking contains an fMet-tRNA^{fMet} that is correctly base paired to a start codon within the 30S IC P site. Driven by this, we assembled and imaged a 30S IC containing IF1, IF2, IF3(Cy3-Cy5) and fMet-tRNA^{fMet} on an mRNA containing an AUG start codon (30S IC^{fMet}) using saturating, 1 μM concentrations of IF1, IF2 and fMet-tRNA^{fMet}. Notably, the average number of surface-tethered, 30S IC^{fMet}–bound IF3(Cy3-Cy5) molecules per field of view did not vary appreciably relative to the number of surface-tethered, 30S IC–bound IF3(Cy3-Cy5) molecules in any of the other identically prepared and imaged 30S ICs we studied. Thus, the presence of an fMet-tRNA^{fMet} that is correctly base paired to a start codon within the P site of 30S IC^{fMet}, at least within the context of the mRNA used here, does not seem to trigger rapid dissociation of IF3 from the 30S IC within the timescale of our experiments (~10 min)[3,5,17]. Instead we found that relative to 30S IC^{-tRNA}, the presence of an fMet-tRNA^{fMet} that is correctly base paired to an AUG start codon within 30S IC^{fMet} shifts the conformational equilibrium of IF3 markedly away from IF3$_{ext}$ and IF3$_{int}$ and toward IF3$_{cpt}$ (**Fig. 3**), yielding fractional occupancies of 15% ± 13% (IF3$_{ext}$), 17% ± 7% (IF3$_{int}$) and 68% ± 17% (IF3$_{cpt}$) (**Supplementary Table 2**). This equilibrium shift seems to be driven primarily by the destabilization of IF3$_{ext}$ and IF3$_{int}$, as evidenced by the large increases in the estimated rates of IF3$_{ext}$→IF3$_{cpt}$ and IF3$_{int}$→IF3$_{cpt}$ transitions in 30S IC^{fMet} relative to 30S IC^{-tRNA} (**Supplementary Table 3**). On the basis of these results, we hypothesized that the observed shift in the conformational equilibrium of 30S IC–bound IF3 toward IF3$_{cpt}$ in 30S IC^{fMet} relative to 30S IC^{-tRNA} forms the molecular and structural basis for signaling fMet-tRNA^{fMet} and start-codon selection within the 30S IC and the associated relaxation of the subunit anti-association activity of IF3. Consistent with this hypothesis, previously reported *in vitro* 50S subunit–joining experiments have shown that 30S ICs analogous to 30S IC^{fMet} undergo rapid 50S subunit joining relative to 30S ICs analogous to 30S IC^{-tRNA} (ref. 4), suggesting that IF3$_{cpt}$ is a conformation of IF3 that is conducive to rapid 50S subunit joining. In the context of this hypothesis, IF3$_{ext}$ and IF3$_{int}$ are not only conformations of IF3 that are not conducive to 50S subunit joining, as discussed above, but also conformations of IF3 that prevent IF3 from populating IF3$_{cpt}$, and consequently from undergoing rapid 50S subunit joining, until the 30S IC has properly selected an fMet-tRNA^{fMet} and the start codon.

The shift toward IF3$_{cpt}$ requires fMet-tRNA^{fMet} and an AUG codon

If the hypothesis outlined in the previous section is correct, then we would expect the shift in the conformational equilibrium of IF3 to depend on the identity of the tRNA and/or codon within the 30S IC P site, as signaling of proper substrate selection and the associated rapid 50S subunit joining occur only within a 30S IC that is specifically carrying an fMet-tRNA^{fMet} that is properly base paired to a start codon. Thus, to further test our hypothesis, we assembled and imaged complete 30S ICs in which the identities of the tRNA and/or codon at the P site were varied. In line with our hypothesis, 30S ICs assembled and imaged using saturating, 1 μM concentrations of either Phe-tRNA^{Phe} or Lys-tRNA^{Lys} and an AUG start codon at the P site (30S IC^{Phe} and 30S IC^{Lys}, respectively) did not undergo the shift in conformational equilibrium of IF3 toward IF3$_{cpt}$ relative to 30S IC^{-tRNA} that we observed for 30S IC^{fMet} relative to 30S IC^{-tRNA} (**Fig. 3**). Instead, the fractional occupancies of IF3$_{ext}$, IF3$_{int}$ and IF3$_{cpt}$ within 30S IC^{Phe} and 30S IC^{Lys} were comparable to those observed within 30S IC^{-tRNA} despite the presence of saturating concentrations of Phe-tRNA^{Phe} or Lys-tRNA^{Lys} (**Fig. 3** and **Supplementary Table 2**). Comparison of 30S IC^{-tRNA}, 30S IC^{fMet}, 30S IC^{Phe} and 30S IC^{Lys} showed that the shift in the conformational equilibrium of IF3 toward IF3$_{cpt}$ depends not only on the presence of an aa-tRNA at the 30S IC P site but also on the identity of that aa-tRNA. Nevertheless, altering the identity of the aa-tRNA, but not the AUG start codon, caused the P sites of 30S IC^{Phe} and 30S IC^{Lys} to contain incorrectly selected elongator aa-tRNAs as well as mismatched GAA-AUG (in the case of 30S IC^{Phe}) and UUU-AUG (in the case of 30S IC^{Lys}) anticodon-codon interactions. Thus, the failure of 30S IC^{Phe} and 30S IC^{Lys} to undergo a shift in the conformational equilibrium of IF3 toward IF3$_{cpt}$ relative to 30S IC^{-tRNA} could potentially be caused by the presence of the elongator aa-tRNA and/or the mismatched anticodon-codon interaction within the 30S IC P site.

To separate the effects that the identity of the aa-tRNA and the nature of the anticodon-codon base-pairing interactions have on the conformational equilibrium of IF3, we imaged completely assembled 30S ICs whose P sites contained either Phe-tRNA^{Phe} at a UUC codon that is cognate for Phe-tRNA^{Phe} (30S IC^{Phe,UUC}) or fMet-tRNA^{fMet} at an AUU codon that is near cognate for fMet-tRNA^{fMet} (30S IC^{fMet,AUU}) using saturating, 1 μM concentrations of Phe-tRNA^{Phe} or fMet-tRNA^{fMet}, respectively. Regardless of the Watson-Crick complementarity of the anticodon-codon interaction in 30S IC^{Phe,UUC}, IF3 showed thermodynamic and kinetic behavior that was comparable to that observed for IF3 within 30S IC^{-tRNA} despite the presence of saturating concentrations of Phe-tRNA^{Phe} (**Fig. 3** and **Supplementary Tables 2** and **3**). Similarly, in the presence of a partially mismatched anticodon-codon interaction in 30S IC^{fMet,AUU}, IF3 showed thermodynamic and kinetic behavior that was comparable to

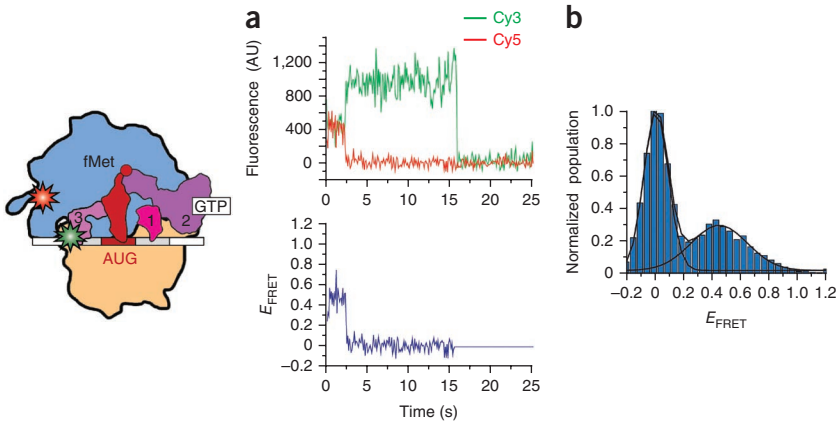

Figure 4 Observation of an intermolecular IF3–50S subunit smFRET signal. The cartoon shows the 70 IC that is formed through stopped-flow delivery of a solution containing 50 nM of the Cy5-labeled 50S subunit (labeled at $L9^{Q18C}$ as previously described)[19] into a flow cell containing a surface-tethered 30S IC^{fMet} carrying $IF3^{C65S\ S38C}$(Cy3), which results in an intermolecular IF3–50S subunit smFRET signal that reports on 50S subunit joining and the formation of a 70S IC. (**a**) A representative example of single-molecule Cy3 (green line) and Cy5 (red line) intensity versus time trajectories (top) and an E_{FRET} versus time trajectory (bottom) for the 70S IC. AU, arbitrary units. (**b**) A normalized, one-dimensional E_{FRET} histogram constructed using the full 120 s of 25 E_{FRET} versus time trajectories. The FRET state centered at an E_{FRET} value of ~0.45 arises from time points in the E_{FRET} versus time trajectories during which the Cy5-labeled 50S subunit has joined to a 30S IC carrying the Cy3-labeled IF3. The FRET state centered at an E_{FRET} value of ~0 arises from time points in the E_{FRET} versus time trajectories before joining of the Cy5-labeled 50S subunit to the 30S IC carrying the Cy3-labeled IF3 and from time points after photobleaching of Cy5 on the Cy5-labeled 50S subunits.

that of 30S IC^{-tRNA} despite the presence of saturating concentrations of fMet-$tRNA^{fMet}$ (**Fig. 3** and **Supplementary Tables 2** and **3**).

DISCUSSION

Taken together, the results we obtained with 30S IC^{Phe}, 30S IC^{Lys}, 30S $IC^{Phe,UUC}$ and 30S $IC^{fMet,AUU}$ suggest that relative to 30S IC^{-tRNA}, the shift in the conformational equilibrium of IF3 toward $IF3_{cpt}$ is dependent on the specific presence of an fMet-$tRNA^{fMet}$ at the 30S IC P site, as well as proper base pairing between fMet-$tRNA^{fMet}$ and a start codon at the P site; these are precisely the conditions under which extensive *in vitro* biochemical experiments have shown that the subunit anti-association activity of IF3 is relaxed and 50S subunit association to the 30S IC is accelerated[4]. Specifically, rapid kinetic experiments have shown that within the context of a 30S IC containing all three initiation factors, the presence of an fMet-$tRNA^{fMet}$ and an AUG start codon increases the rate of 50S subunit joining by a factor of 1,200 relative to a 30S IC lacking an aa-tRNA at the P site[4], a factor of 400 relative to a 30S IC carrying a Phe-$tRNA^{Phe}$ that is mismatched to an AUG start codon[2] and a factor of 90 relative to a 30S IC carrying an fMet-$tRNA^{fMet}$ that is mismatched to a noncanonical start codon[5].

Integrating our current findings regarding the conformational dynamics of 30S IC–bound IF3 with the results of the biochemical studies described in the previous paragraph allows us to propose a structure-based mechanistic model for how IF3 recognizes and signals fMet-$tRNA^{fMet}$ and start-codon selection within the 30S IC to gate further progress along the initiation pathway. In our model, 30S IC–bound IF3 can sample at least three major conformations, $IF3_{ext}$, $IF3_{int}$ and $IF3_{cpt}$, whose thermodynamic stabilities respond strongly to the composition of the 30S IC. In 30S ICs carrying all three initiation factors but lacking an aa-tRNA, carrying an elongator aa-tRNA or carrying an

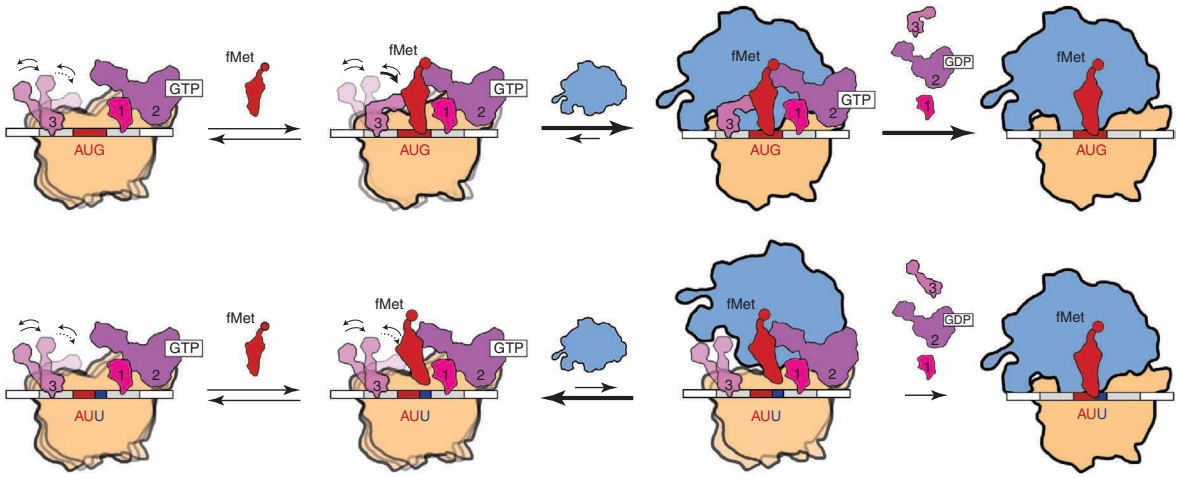

Figure 5 A structure-based mechanistic model for how IF3 recognizes and signals fMet-$tRNA^{fMet}$ and start-codon selection within the 30S IC. 30S IC–bound IF3 exists in a conformational equilibrium in which it can dynamically exchange between at least three distinct conformational states, $IF3_{ext}$, $IF3_{int}$ and $IF3_{cpt}$. Specific recognition of an fMet-$tRNA^{fMet}$ that is properly base paired to a start codon within the P site of a 30S IC carrying all three initiation factors shifts the conformational equilibrium of IF3 strongly toward $IF3_{cpt}$, a conformation of 30S IC–bound IF3 that exposes and/or optimally positions ribosomal RNA and/or ribosomal protein residues on the 30S IC that are crucial for intersubunit bridge formation and is thus conducive to rapid and productive 50S subunit joining (top). In contrast, the absence of an aa-tRNA, the presence of an elongator aa-tRNA or the presence of a noncanonical start codon within the P site of a 30S IC carrying all three initiation factors shifts the conformational equilibrium of IF3 strongly toward $IF3_{ext}$ and $IF3_{int}$, conformations of 30S IC–bound IF3 that occlude and/or misorient residues involved in intersubunit bridge formation and are thus not conducive to efficient 50S subunit joining (bottom).

fMet-tRNA^{fMet} that is mismatched to a noncanonical start codon within the 30S IC P site, the conformational equilibrium of IF3 is strongly shifted toward IF3$_{ext}$ and IF3$_{int}$, which are conformations of IF3 that are not conducive to rapid 50S subunit joining. Specific recognition of an fMet-tRNA^{fMet} that is properly base paired to a start codon within the P site of a 30S IC carrying all three initiation factors, in contrast, strongly shifts the conformational equilibrium of IF3 toward IF3$_{cpt}$, which is a conformation of IF3 that signals proper substrate selection and is conducive to rapid 50S subunit joining. It is interesting that IF3 predominantly occupies IF3$_{cpt}$ in both the completely and correctly assembled 30S IC (30S IC^{fMet}) as well as the incompletely assembled 30S IC lacking IF1 and fMet-tRNA^{fMet} (30S IC$_{-1}^{-tRNA}$) (**Figs. 2b** and **3**). Thus, in the absence of IF1 and fMet-tRNA^{fMet}, the presence of IF2 on the 30S IC can shift the conformational equilibrium of IF3 toward IF3$_{cpt}$. This is notable in light of rapid kinetic data indicating that 50S subunit joining to a 30S IC that is analogous to 30S IC$_{-1}^{-tRNA}$ is 145-fold slower than joining to a 30S IC that is analogous to 30S IC^{fMet} (ref. 3). Thus, although our model stipulates that IF3$_{cpt}$ is conducive to and permits rapid 50S subunit joining, it is probable that additional factors, such as the presence of IF2 and fMet-tRNA^{fMet} on the 30S IC[2,3], are required to actualize rapid 50S subunit joining. Furthermore, the finding that IF3$_{cpt}$ is rarely sampled within 30S IC^{-tRNA} suggests that IF1 has a key role in negatively regulating the conformational dynamics of IF3 such that 30S IC–bound IF3 does not substantially populate IF3$_{cpt}$ in the absence of fMet-tRNA^{fMet} that is correctly base paired to a start codon.

Although we will have to wait until X-ray crystallographic structures of the 30S IC are solved to confirm our suspicions, we suspect that IF3$_{cpt}$ is a conformation of 30S IC–bound IF3 that exposes and/or optimally positions ribosomal RNA and/or ribosomal protein residues on the 30S IC that are crucial for intersubunit bridge formation, thus enabling rapid and productive 50S subunit joining, whereas IF3$_{ext}$ and IF3$_{int}$ are conformations of 30S IC–bound IF3 that occlude and/or misorient these residues, thereby blocking 50S subunit joining. In contrast with models in which a selective increase in the rate of spontaneous dissociation of IF3 from the 30S IC is required for productive 50S subunit joining[3], the model presented here predicts that efficient 50S subunit joining can occur on a completely and correctly assembled 30S IC that contains IF3. Indeed, preliminary smFRET data collected using Cy3-labeled IF3 and Cy5-labeled 50S subunits (labeled at ribosomal protein L9) revealed that the 50S subunit can rapidly and productively join to a completely and correctly assembled 30S IC containing IF3 that is presumably in the IF3$_{cpt}$ conformation (30S IC^{fMet}) (**Fig. 4**). Nevertheless, our model (**Fig. 5**) and intermolecular 50S-IF3 smFRET data do not exclude the possibility that IF3 in the IF3$_{cpt}$ conformation is more weakly bound to the 30S IC than is IF3 in the IF3$_{ext}$ and IF3$_{int}$ conformations, such that IF3 in the IF3$_{cpt}$ conformation is easily displaced from the 30S IC during or shortly after productive 50S subunit joining. Indeed, kinetic measurements[5,18] have suggested that 50S subunit joining to the 30S IC is slightly faster than the rate of IF3 dissociation from the 30S IC. Given recent studies demonstrating that differences in the translation initiation region of individual mRNAs, such as the sequence of the Shine-Dalgarno element and the length of the spacer between the Shine-Dalgarno element and the start codon, can influence the rate of 50S subunit joining to 30S ICs assembled on different mRNAs[5,17], it is possible that translation initiation region–mediated regulation of the conformational equilibrium of 30S IC–bound IF3 will be an effective mechanism for regulating the efficiency with which individual mRNAs are initiated and translated in the cell.

METHODS

Methods and any associated references are available in the online version of the paper.

Note: Supplementary information is available in the online version of the paper.

ACKNOWLEDGMENTS

We thank M.A. Gawinowicz for performing trypsin digestion and MALDI-TOF mass spectrometry analysis of IF3(Cy3-Cy5), D. MacDougall for assistance with protein purification and J.W. van de Meent for assistance with smFRET data analysis. We also thank members of the Gonzalez research group, especially D. MacDougall, J. Wang, K. Caban and C. Kinz-Thompson, for discussions and comments on the manuscript. Financial support for this work was provided by Career Award in the Biomedical Sciences 1004856 from the Burroughs Wellcome Fund (R.L.G.), Research Project Grant GM084288 from the US National Institutes of Health (R.L.G.) and Molecular Biophysics Training Grant T32GM008281 from the US National Institutes of Health (M.M.E.).

AUTHOR CONTRIBUTIONS

M.M.E. and R.L.G. contributed to the experimental design, data interpretation and manuscript writing. M.M.E. performed the experiments and carried out data analyses.

COMPETING FINANCIAL INTERESTS

The authors declare no competing financial interests.

1. Laursen, B.S., Sorensen, H.P., Mortensen, K.K. & Sperling-Petersen, H.U. Initiation of protein synthesis in bacteria. *Microbiol. Mol. Biol. Rev.* **69**, 101–123 (2005).
2. Antoun, A., Pavlov, M.Y., Lovmar, M. & Ehrenberg, M. How initiation factors maximize the accuracy of tRNA selection in initiation of bacterial protein synthesis. *Mol. Cell* **23**, 183–193 (2006).
3. Antoun, A., Pavlov, M.Y., Lovmar, M. & Ehrenberg, M. How initiation factors tune the rate of initiation of protein synthesis in bacteria. *EMBO J.* **25**, 2539–2550 (2006).
4. Antoun, A., Pavlov, M.Y., Tenson, T. & Ehrenberg, M. Ribosome formation from subunits studied by stopped-flow and Rayleigh light scattering. *Biol. Proced. Online* **6**, 35–54 (2004).
5. Milon, P., Konevega, A.L., Gualerzi, C.O. & Rodnina, M.V. Kinetic checkpoint at a late step in translation initiation. *Mol. Cell* **30**, 712–720 (2008).
6. de Cock, E., Springer, M. & Dardel, F. The interdomain linker of *Escherichia coli* initiation factor IF3: a possible trigger of translation initiation specificity. *Mol. Microbiol.* **32**, 193–202 (1999).
7. Moreau, M. *et al.* Heteronuclear NMR studies of *E. coli* translation initiation factor IF3. Evidence that the inter-domain region is disordered in solution. *J. Mol. Biol.* **266**, 15–22 (1997).
8. Dallas, A. & Noller, H.F. Interaction of translation initiation factor 3 with the 30S ribosomal subunit. *Mol. Cell* **8**, 855–864 (2001).
9. Julián, P. *et al.* The cryo-EM structure of a complete 30S translation initiation complex from *Escherichia coli*. *PLoS Biol.* **9**, e1001095 (2011).
10. McCutcheon, J.P. *et al.* Location of translational initiation factor IF3 on the small ribosomal subunit. *Proc. Natl. Acad. Sci. USA* **96**, 4301–4306 (1999).
11. Fabbretti, A. *et al.* The real-time path of translation factor IF3 onto and off the ribosome. *Mol. Cell* **25**, 285–296 (2007).
12. Murphy, M.C., Rasnik, I., Cheng, W., Lohman, T.M. & Ha, T. Probing single-stranded DNA conformational flexibility using fluorescence spectroscopy. *Biophys. J.* **86**, 2530–2537 (2004).
13. Bastiaens, P.I. & Jovin, T.M. Microspectroscopic imaging tracks the intracellular processing of a signal transduction protein: fluorescent-labeled protein kinase C β I. *Proc. Natl. Acad. Sci. USA* **93**, 8407–8412 (1996).
14. Adcock, S.A. & McCammon, J.A. Molecular dynamics: survey of methods for simulating the activity of proteins. *Chem. Rev.* **106**, 1589–1615 (2006).
15. Maar, D. *et al.* A single mutation in the IF3 N-terminal domain perturbs the fidelity of translation initiation at three levels. *J. Mol. Biol.* **383**, 937–944 (2008).
16. Howe, J.G. & Hershey, J.W. Initiation factor and ribosome levels are coordinately controlled in *Escherichia coli* growing at different rates. *J. Biol. Chem.* **258**, 1954–1959 (1983).
17. Milón, P., Maracci, C., Filonava, L., Gualerzi, C.O. & Rodnina, M.V. Real-time assembly landscape of bacterial 30S translation initiation complex. *Nat. Struct. Mol. Biol.* **19**, 609–615 (2012).
18. Grigoriadou, C., Marzi, S., Pan, D., Gualerzi, C.O. & Cooperman, B.S. The translational fidelity function of IF3 during transition from the 30 S initiation complex to the 70 S initiation complex. *J. Mol. Biol.* **373**, 551–561 (2007).
19. Fei, J. *et al.* Allosteric collaboration between elongation factor G and the ribosomal L1 stalk directs tRNA movements during translation. *Proc. Natl. Acad. Sci. USA* **106**, 15702–15707 (2009).

ONLINE METHODS

Sample preparation. *E. coli* ribosomes and translation factors were purified as previously described[20]. 5′-biotinylated mRNA with a sequence derived from the mRNA encoding gene product 32 from T4 bacteriophage was purchased from Dharmacon, Inc. See the **Supplementary Note** for details on the sequence of this mRNA. $tRNA^{fMet}$ was purchased from MP Biomedicals, and $tRNA^{Phe}$ and $tRNA^{Lys}$ were purchased from Sigma. All tRNAs were aminoacylated and, in the case of $tRNA^{fMet}$, formylated as previously described[20].

The gene encoding *E. coli* IF3 was cloned into the pProEx-HTb plasmid vector (Invitrogen), which encodes a hexahistidine (His_6) affinity purification tag and a TEV protease cleavage site at the N-terminal end of the gene encoding IF3. Mutagenesis of IF3 in the pProEx-HTb plasmid vector was performed using the QuikChange Site-Directed Mutagenesis System (Stratagene). DNA primers for mutagenesis were designed following the recommendations provided by the QuikChange Site-Directed Mutagenesis System and were purchased from Integrated DNA Technologies. No further purification of the DNA primers was performed. Using this approach, the single Cys65 in wild-type IF3 was mutagenized to serine, Ser38 in the NTD was mutagenized to cysteine, and Lys97 in the CTD was mutagenized to cysteine, yielding a triple-mutant IF3 variant ($IF3^{C65S\ S38C\ K97C}$). Note that the residue numbering for IF3 used in this study is based on wild-type *E. coli* IF3 numbering. Mutations were verified by DNA sequencing of the plasmid purified from an ampicillin-resistant clone (Genewiz). The pProEx-HTb plasmids encoding all of the IF3 variants used in this study were transformed into BL21-DE3 cells for protein overexpression, and the overexpressed His_6-tagged IF3 variants were purified using Ni^{2+}–nitrilotriacetic acid affinity purification, treated with TEV protease to remove the His_6 tags and further purified using cation exchange chromatography. Further details regarding the cloning, overexpression and purification of the IF3 variants used in this study can be found in ref. 20. The N terminus of the IF3 variants used in this study consists of a GlyAlaMetAlaLys2 sequence, where GlyAlaMetAla denotes four non–wild type amino acids resulting from the cloning strategy, and Lys2 denotes the beginning of the wild-type *E. coli* IF3 sequence.

$IF3^{C65S\ S38C\ K97C}$ was labeled with Cy3- and Cy5-maleimide (GE Healthcare) following the manufacturer's recommendations. See the **Supplementary Note** for further details.

The unlabeled, monolabeled and dual-labeled $IF3^{C65S\ S38C\ K97C}$ products were separated using a TSKgel Phenyl-5PW hydrophobic interaction chromatography (HIC) column (Tosoh Bioscience) that had been pre-equilibrated with HIC Buffer A (**Supplementary Table 4**). A 0–100% linear gradient of HIC Buffer B applied over 20 column volumes enabled separation of the various unlabeled and labeled IF3 species (**Supplementary Fig. 1**).

The biochemical activities of mutagenized and fluorescently labeled $IF3^{C65S\ S38C\ K97C}$ (IF3(Cy3-Cy5)) and $IF3^{C65S\ S38C\ K97C\ Y75N}$ ($IF3^{Y75N}$(Cy3-Cy5)) were tested using a primer extension inhibition, or toeprinting, assay and a TIRF microscopy–based tRNA dissociation assay (**Supplementary Fig. 2**).

30S ICs for smFRET studies were prepared by incubating 1.8 μM 5′-biotinylated mRNA, 0.9 μM IF1, 0.9 μM IF2, 0.9 μM tRNA, 0.6 μM 30S subunits and 0.6 μM IF3(Cy3-Cy5) at 37 °C for 10 min in Tris-Polymix buffer (**Supplementary Table 4**). 30S ICs were then aliquoted, flash frozen in liquid nitrogen and stored at −80 °C until further use.

TIRF microscopy. 30S ICs for imaging by TIRF microscopy were thawed, diluted to ~200 pM in Tris-Polymix buffer (**Supplementary Table 4**), introduced into a microfluidic flow cell that had been passivated with a mixture of polyethylene glycol and biotinylated PEG and derivatized with streptavidin as previously described[21], and incubated at room temperature for 5 min. 30S ICs that did not tether to the surface of the flow cell at the end of the 5-min incubation were removed by flushing the flow cell with Tris-Polymix buffer containing an enzymatic oxygen scavenger system, a triplet-state quencher cocktail and, as specified in the individual experiments, mixtures of initiation factors and aa-tRNAs (**Supplementary Table 4**).

A previously described, laboratory-built, wide-field, prism-based TIRF microscope[22] was used to image the flow cells containing the surface-tethered 30S ICs. Briefly, a diode-pumped, solid-state, 532-nm laser (CrystaLaser) operating at a power of 7 mW (measured just before striking the prism) was used to directly excite Cy3, and a diode-pumped, solid-state, 643-nm laser (CrystaLaser) operating at a power of 18 mW (measured just before striking the prism) was used to directly excite Cy5. Fluorescence emissions from Cy3 and Cy5 were collected through a high numerical aperture objective (Nikon), wavelength separated into individual Cy3 and Cy5 fields of view using a Dual-View simultaneous imaging system (Photometrics, Inc.) and simultaneously imaged using the two halves of a back-thinned, 512 pixel × 512 pixel electron-multiplying charged-coupled device (EMCCD) camera (Cascade II 512:B, Photometrics, Inc.) operating with 2 pixel × 2 pixel binning and a frame rate of 10 frames s^{-1}.

Within a 60 μm × 120 μm field of view, 200–400 spatially well separated 30 ICs were imaged. Direct excitation of Cy5 using the 643-nm laser during the first frame of each movie was used to record the spatial location of each Cy5 fluorophore in the field of view. The 643-nm laser was subsequently switched off and the 532-nm laser was switched on simultaneously to directly excite Cy3 and perform smFRET imaging starting with the second frame of each movie. Imaging continued until >95% of the Cy3 fluorophores had photobleached. Three independent data sets consisting of 12–15 movies each were collected on separate days using independently prepared samples and microfluidic devices for each 30S IC.

smFRET data analysis. Generation and selection of single-molecule E_{FRET} versus time trajectories from each movie were performed as previously described[19,21,23]. Briefly, the first frame of each movie, which was collected using direct excitation of Cy5 with a 643-nm laser, was used to identify single, diffraction-limited Cy5 spots. The locations of these spots were transferred to the Cy3 field of view to align the Cy5 field of view with the subsequent 532 nm–directly excited Cy3 field of view. The aligned Cy3 and Cy5 fields of view were used to identify pairs of Cy3 and Cy5 spots corresponding to single, surface-tethered 30S ICs carrying dual Cy3-Cy5–labeled IF3s, and MetaMorph (Molecular Devices), Excel (Microsoft), Origin (OriginLab Corporation) and Matlab (The MathWorks) were used to plot Cy3 and Cy5 intensity versus time trajectories for each IF3. Trajectories with (i) time-averaged Cy3 and Cy5 intensity values characteristic of single Cy3 and Cy5 fluorophores, respectively, as determined by visual inspection; (ii) single-step photobleaching of Cy3 and/or Cy5 fluorophores, as determined by visual inspection; (iii) anticorrelated changes in Cy3 and Cy5 intensities, as determined by visual inspection; and (iv) Cy5 fluorescence lasting longer than 1 s before photobleaching, as determined by visual inspection, were kept for further analysis (see **Fig. 2a** for representative Cy3 and Cy5 versus time trajectories). In addition to these selection criteria, trajectories in which FRET could not be confirmed because of the simultaneous, single-step drop of both Cy3 and Cy5 intensities to baseline before undergoing an anticorrelated change in Cy3 and Cy5 intensities (<10% of the total number of trajectories per independently collected data set) were omitted from further analysis. Each of the Cy3 and Cy5 versus time trajectories selected for further analysis was baseline corrected by subtracting the average EMCCD readout over the last ten Cy3 time points (that is, after photobleaching of the Cy3 fluorophore) from each Cy3 time point and subtracting the average EMCCD readout over the last ten Cy5 time points (that is, after photobleaching of the Cy5 fluorophore) from each Cy5 time point. In addition, each Cy5 time point was corrected for bleed through of Cy3 intensity into the Cy5 field of view, which arises from the imperfect performance of emission filters, by subtracting 7% of the total Cy3 intensity (the experimentally determined average amount of Cy3 intensity that bleeds through into the Cy5 field of view in our TIRF microscope system) at each time point from the Cy5 intensity at the same time point. Each pair of baseline-corrected and bleed through–corrected Cy3 and Cy5 versus time trajectories was converted to a single, raw E_{FRET} versus time trajectory using the equation $E_{FRET} = I_{Cy5}/(I_{Cy3} + I_{Cy5})$, where E_{FRET} is the FRET efficiency at each time point and I_{Cy3} and I_{Cy5} are the baseline-corrected and bleed through–corrected Cy3 and Cy5 intensities at each time point, respectively. The raw E_{FRET} versus time trajectories were idealized by hidden Markov modeling using the vbFRET software package[24] and further analyzed as described in **Figure 2** and **Supplementary Tables 1–3**. All data are presented as the mean ± s.d.

20. Fei, J. *et al.* A highly purified, fluorescently labeled *in vitro* translation system for single-molecule studies of protein synthesis. *Methods Enzymol.* **472**, 221–259 (2010).

doi:10.1038/nsmb.2554

21. Fei, J., Kosuri, P., MacDougall, D.D. & Gonzalez, R.L. Jr. Coupling of ribosomal L1 stalk and tRNA dynamics during translation elongation. *Mol. Cell* **30**, 348–359 (2008).
22. Blanchard, S.C., Kim, H.D., Gonzalez, R.L. Jr., Puglisi, J.D. & Chu, S. tRNA dynamics on the ribosome during translation. *Proc. Natl. Acad. Sci. USA* **101**, 12893–12898 (2004).
23. Sternberg, S.H., Fei, J., Prywes, N., McGrath, K.A. & Gonzalez, R.L. Jr. Translation factors direct intrinsic ribosome dynamics during translation termination and ribosome recycling. *Nat. Struct. Mol. Biol.* **16**, 861–868 (2009).
24. Bronson, J.E., Fei, J., Hofman, J.M., Gonzalez, R.L. Jr. & Wiggins, C.H. Learning rates and states from biophysical time series: a Bayesian approach to model selection and single-molecule FRET data. *Biophys. J.* **97**, 3196–3205 (2009).